Acta Chemica Scandinavica A 38 (1984) 703–710

Magnetic and Structural Properties of Transition Metal Substituted MnP. II. $Mn_{1-t}V_tP$ ($0.00 \leqq t \leqq 0.25$)

HELMER FJELLVÅG and ARNE KJEKSHUS

Kjemisk Institutt, Universitetet i Oslo, Blindern, N-0315 Oslo 3, Norway

$Mn_{1-t}V_tP$ is studied for $0.00 \leqq t \leqq 0.25$ by X-ray and neutron diffraction below and above room temperature. Magnetic susceptibility data for the same samples are also included. The MnP type atomic arrangement prevails under these conditions in para-, ferro- or helimagnetic states. The results are discussed in relation to other information on $Mn_{1-t}V_tP$ and related phases.

The current interest in the $Mn_{1-t}T_tP$ (T=transition metal) and $MnP_{1-x}X_x$ (X=metalloid) phases originates from the rather unique magnetic properties of MnP (*cf.* Ref. 1 and references therein). The solid solution phases have opened for additional opportunities to study more and further details of the properties of MnP. In addition, the properties of $Mn_{1-t}T_tP$ and $MnP_{1-x}X_x$ are interesting in their own right.

The structural and magnetic properties of $Mn_{1-t}Co_tP$ are considered in the preceeding paper[2] of this series, and discussed in relation to the properties of MnP itself. The present contribution concerns $Mn_{1-t}V_tP$, properties of which have also been disclosed in earlier communications.[3,4]

EXPERIMENTAL

Samples were made from initial batches of MnP and VP (preparational details, including purity of elements are given in Refs. 2–4) by a first heat treatment at 1000 °C for 5 d. All samples (t=0.05, 0.10, 0.15, 0.20 and 0.25) were ground and subjected to two further heat treatments (intermediate grinding) for 5 d at 1000 °C, before finally being cooled slowly to room temperature over 1 d.

The experimental details concerning powder X-ray and neutron diffraction are given in Ref. 5. The nuclear neutron scattering lengths (in 10^{-12} cm) $b_V=-0.038$, $b_{Mn}=-0.37$ and $b_p=0.51$ were taken from Ref. 6, and the magnetic form factor for Mn^{2+} from Ref. 7.

RESULTS AND DISCUSSION

(i) *Atomic arrangement.* In conformity with Ref. 3, $Mn_{1-t}V_tP$ with $0.00 \leqq t \leqq 0.25$ exhibits the MnP type atomic arrangement (here using *Pnma* setting, $c>a>b$) at, and below, room temperature. The generally sharp Bragg reflections together with the lack of additional superstructure reflections in the X-ray and neutron diffraction diagrams confirm that Mn and V are randomly (long range) distributed over the metal sub-lattice. The unit cell dimensions and positional parameters, as derived from powder neutron diffraction data, are listed in Table 1.

The unit cell dimensions of $Mn_{1-t}V_tP$ *versus* t ($0.00 \leqq t \leqq 0.25$) at 10 and 293 K in Fig. 1 go well together with the corresponding room temperature data in Ref. 3. The slightly larger scatter of the neutron (compared with the X-ray) diffraction points in Fig. 1 originates from the methodology of the former technique. As pointed out in Refs. 2, 5, an expansion of the b axis with decreasing temperature can be used as an indicator of ferro- (F) and/or helimagnetic (H_c) states. The reversal of b between 293 and 10 K for $0.00 \leqq t \leqq \sim 0.20$ in Fig. 1 thus concurs with the fact that this is just the domain of the F and H_c phases of $Mn_{1-t}V_tP$ [see (iii) and Ref. 4].

The thermal expansion curves for t=0.05, 0.10 and 0.20 (Fig. 2) also contain some indications of

0302-4377/84 $2.50

Table 1. Unit cell dimensions and positional parameters with standard deviations for $Mn_{1-t}V_tP$ as derived by Rietveld analysis of powder neutron diffraction data. Space group *Pnma*; Mn/V in 4*c* and P in 4*c*. (Nuclear R_n-factors ranging between 0.03 and 0.07; magnetic R_m-factors ranging between 0.03 and 0.08; profile R_p-factors ranging between 0.08 and 0.13; 20–25 nuclear reflections.)

t	T (K)	*a* (pm)	*b* (pm)	*c* (pm)	x_T	z_T	x_P	z_P
0.05	293	526.43(5)	316.87(2)	592.32(5)	0.0074(26)	0.1949(25)	0.1880(17)	0.5682(14)
	100	524.62(7)	317.38(4)	590.80(8)	0.0032(30)	0.1939(35)	0.1893(22)	0.5691(19)
	10	524.57(6)	317.41(3)	590.67(6)	0.0063(31)	0.1986(31)	0.1865(21)	0.5694(17)
0.10	293	528.75(5)	317.06(3)	594.84(6)	0.0063(21)	0.1979(26)	0.1879(16)	0.5684(14)
	160	527.20(5)	317.13(3)	593.44(6)	0.0083(28)	0.1961(28)	0.1876(18)	0.5683(15)
	140	526.63(7)	316.93(3)	592.67(8)	0.0079(34)	0.1953(35)	0.1882(22)	0.5678(18)
	10	526.47(6)	317.06(3)	592.53(6)	0.0066(34)	0.1953(34)	0.1876(22)	0.5679(18)
0.15	293	530.40(4)	316.43(2)	596.61(4)	0.0046(14)	0.1969(13)	0.1874(8)	0.5674(7)
	10	528.58(4)	316.45(2)	594.79(4)	0.0043(15)	0.1969(14)	0.1869(9)	0.5688(7)
0.20	293	531.82(4)	316.27(2)	598.13(2)	0.0061(14)	0.1961(13)	0.1878(8)	0.5676(6)
	10	530.31(4)	316.12(2)	596.09(5)	0.0031(17)	0.1948(15)	0.1856(9)	0.5675(7)
0.25	293	532.67(5)	316.01(3)	598.76(6)	0.0077(28)	0.1970(24)	0.1882(14)	0.5669(11)
	10	531.23(4)	315.51(2)	597.41(5)	0.0086(24)	0.1947(21)	0.1848(13)	0.5665(11)

Fig. 1. Unit cell dimensions of $Mn_{1-t}V_tP$ at 10 and 293 K as functions of t ($0.00 \leqq t \leqq 0.25$). Legends to symbols are given on the illustration. *Calculated* error limits do not exceed twice the size of symbols. (1 Å=10^2 pm.)

the P (paramagnetic)$\rightleftarrows$F transition, but these data only provide inaccurate values for T_C. Hence, this technique is less successful for $Mn_{1-t}V_tP$ than was the case for *e.g.* $Mn_{1-t}Cr_tAs$.[5] This is partly due to the methodology and partly a consequence of the combined effects of magnetostriction and thermal expansion/contraction for the particular case. The occurrence of magnetostriction is clearly noticeable in the thermal behaviour of the *b* axis (Fig. 2).

The positional parameters of $Mn_{1-t}V_tP$ (Table 1) are constant within two calculated standard

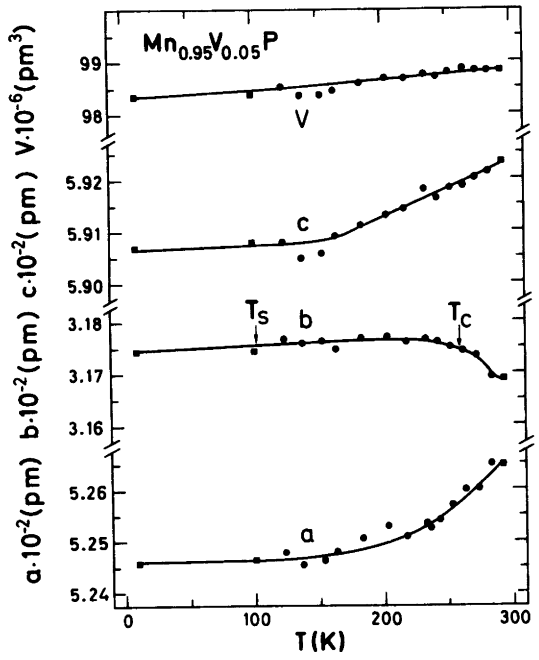

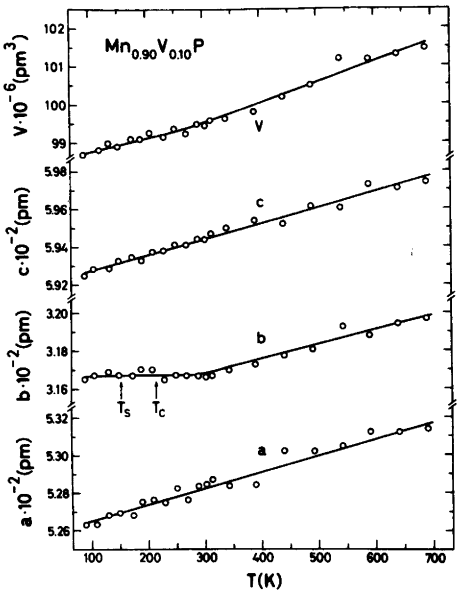

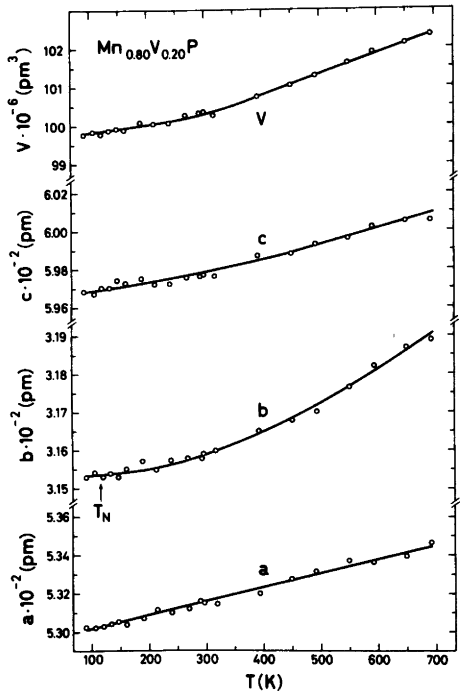

Fig. 2. Unit cell dimensions *versus* temperature ($T<300$ K) for (a) $Mn_{0.95}V_{0.05}P$, (b) $Mn_{0.90}V_{0.10}P$ and (c) $Mn_{0.80}V_{0.20}P$. *Calculated* error limits do not exceed the size of symbols. Circles and squares represent results derived from X-ray and neutron diffraction data, respectively. (1 Å=10^2 pm.) T_C, T_N and T_S refer to the P⇆F, P⇄H_c and F to H_c transition temperatures, respectively, given in (iii).

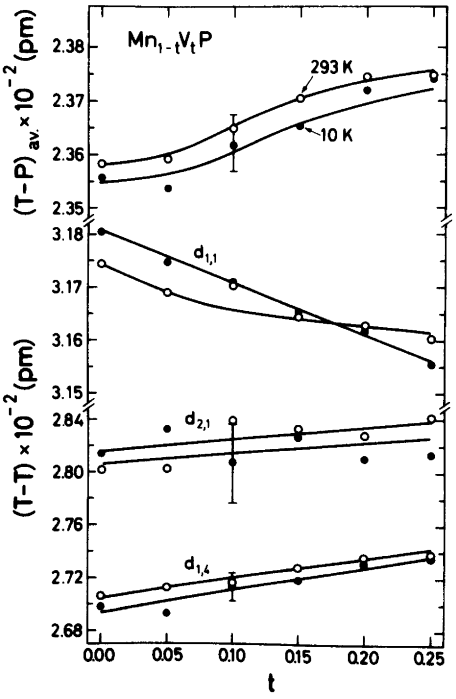

Fig. 3. Interatomic distances ($T-T$, average $T-P$) at 10 and 293 K as functions of t in $Mn_{1-t}V_tP$. T denotes here average Mn, V. Indices i,j on the $T-T$ distances ($d_{i,j}$) refer to the numbering of T given in Ref. 5. Error bars are derived from the calculated, maximum standard deviations. Concerning the curves see the text.

deviations for $0.00 \leqq t \leqq 0.25$ and $10 \leqq T \leqq 293$ K. This result concurs with the findings for other $Mn_{1-t}T_tP$ phases[2,8] and the geometrical considerations in Refs. 9, 10 (taking into account that $Mn_{1-t}V_tP$ with $0.00 \leqq t \leqq \sim 0.75$ probably retains the MnP type structure up to the melting point).

The compositional variations at 10 and 293 K of the average metal–phosphorous and the three shortest metal–metal interatomic distances in $Mn_{1-t}V_tP$ (as derived from the data in Table 1) are shown in Fig. 3. As seen from the error bars shown on the illustration, the second shortest metal–metal distance ($d_{2,1}$ which corresponds to zig-zag chains along the b direction) is particularly hampered by the inaccuracies in the positional parameters. On the other hand, the third shortest metal–metal distance ($d_{1,1}$) equals the b axis and is accordingly very precisely determined. On the basis of the experimental points and error bars in Fig. 3 only $d_{1,1}$ is subject to a significant change between 10 and 293 K. However, the clear-cut trend for the average metal–phosphorous distance suggests that also this quantity is temperature dependent. Smaller temperature and concentration variations can easily be masked by the scatter of the positional parameters within their appreciable standard deviations. Since the positional parameters show indications of invariability with respect to T and t, their averages were combined with the observed unit cell dimensions (Table 1) to generate interatomic distances on this basis. The resulting curves in Fig. 3 show that this procedure (as expected) closely simulates the points, thus emphasizing the correlation to unit cell dimensions in such cases. We intend to return to this aspect in a broader context.

(ii) *Magnetic susceptibility.* The reciprocal magnetic susceptibility *versus* temperature characteristics for $Mn_{1-t}V_tP$ with $0.00 \leqq t \leqq 0.30$ in Ref. 3 differ from those for other, corresponding-

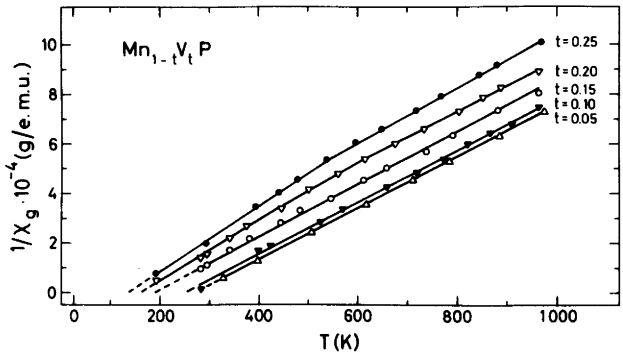

Fig. 4. Inverse magnetic susceptibility as function of temperature for $Mn_{1-t}V_tP$ with t=0.05, 0.10, 0.15, 0.20 and 0.25.

ly diluted $Mn_{1-t}T_tP$ phases[3,8,11] by their non-linear (slightly sigmoidal) shape. Hence, the χ^{-1} (T) curves for the present neutron diffraction samples were recorded, and the results in Fig. 4 show that also $Mn_{1-t}V_tP$ indeed falls nicely into the general pattern. Since, renewed measurements on the samples used in Ref. 3 confirm the earlier findings, there had to be a distinction between the two sets of samples. Even very careful examination by the X-ray (Guinier) diffraction technique failed to bring out any such distinction. However, analyses of a few samples by Auger and/or ESCA show clear-cut evidence of surface oxidation. The surface oxidation appears indeed to be more severe for the samples of Ref. 3 than for the present samples, but we were unfortunately unable to pursue the problem further.

The χ^{-1}(T) curves for $Mn_{1-t}V_tP$ (Fig. 4; see Ref. 3 for $t \geqq 0.40$, the magnetic consequences of the oxidation being evidently less important for V rich samples) show a gradual change in character. The straight lines for low substitution levels of V, convert to curves which are concave towards the temperature axis when the V content increases. This trend concurs with the findings for all $Mn_{1-t}T_tP$ phases[3,8,11] which we have examined.

The χ^{-1}(T) curves for t=0.05, 0.10 and 0.15 fulfil Curie-Weiss law [$\chi^{-1}=C^{-1}(T-\theta)$] for the entire temperature interval shown in Fig. 4 whereas those for t=0.20 and 0.25 can be approximated by two such relationships. The paramagnetic moment ($\mu_{eff}=[8C_{mol}]^{1/2}$) and Weiss constant ($\theta$) as derived from the Curie-Weiss regions are listed in Table 2, which also includes the number of unpaired spins ($2S$) according to the "spin only" approximation ($\mu_{eff}=g[S(S+1]^{1/2}$ with g=2). The data for the "low" temperature Curie-Weiss regions reveal a decline in θ, μ_{eff} and $2S$, whereas the "high" temperature regions lead to appreciably lower values for θ and roughly concentration independent μ_{eff} and $2S$. However, judging from the general trend in the shape of the χ^{-1}(T) curves of $Mn_{1-t}T_tP$ it seems likely that parameters derived from the "high temperature Curie-Weiss regions" have no physical significance. This problem will in any case be left open in this context.

The θ values for $Mn_{1-t}V_tP$ with t=0.05 and 0.10 concur with the Curie temperatures (T_C) derived by neutron diffraction and/or magnetization measurements, whereas those for t=0.15 and 0.20 fall above the Néel temperatures (T_N) determined by neutron diffraction [see (iii) and Ref. 4]. These findings are as expected since T_C and θ normally agree within some 20 K as opposed to T_N and θ which may differ appreciably depending on the number and kinds of magnetic exchange interactions involved. The MnP,H_c type magnetic structure is indeed governed by several different exchange interactions (*cf., e.g.,* Refs. 12, 13). The relation between $2S$ and the magnetic moments deduced by neutron diffraction and magnetization measurements [see (iii) and Ref. 4] is shown in Fig. 5. As seen from the illustration there is an almost perfect match between the extrapolated magnetization moments and the helimagnetic moments (μ_H). In line with the findings for all $Mn_{1-t}T_tP$ (and other) phases the paramagnetic $2S$ values are considerably higher than the ordered moments μ, but both curves in Fig. 5 show a decrease with increasing t. These aspects will be discussed in relation to the corresponding data for all $Mn_{1-t}T_tP$ phases.[8]

Table 2. Weiss constant (θ), paramagnetic moment (μ_{eff}) and number of unpaired spins ($2S$) for $Mn_{1-t}V_tP$.

t	θ (K)	μ_{eff} (μ_B per T)	2S (per T)
0.05	265±10	2.59±0.10	1.77±0.08
0.10	250±10	2.56±0.10	1.75±0.08
0.15	185±10	2.51±0.10	1.70±0.08
0.20[a]	160±15	2.38±0.15	1.58±0.12
0.20[b]	85±15	2.59±0.15	1.77±0.12
0.25[a]	135±15	2.27±0.15	1.48±0.12
0.25[b]	55±15	2.48±0.15	1.67±0.12

[a] For T<~450 K. [b] For T>~450 K.

(iii) *Magnetic structures.* The magnetic phase diagram for $Mn_{1-t}V_tP$ for $0.00 \leqq t \leqq 0.50$ and 0<T<300 K in Ref. 4 comprises in addition to the P, F and H_c phases a spin glass (SG) region for $\sim 0.30 < t < \sim 0.50$. The present data were taken into account when the diagram was prepared.

By the neutron diffraction technique, the occurrence of the F phase could only be unequivocally established for t=0.05, T_C=260±5 K, $\mu_F \approx 0.8\ \mu_B$ (direction of moments parallel to b) at 160 K. The neutron diffraction diagrams for t=0.10 between 200 and 160 K also gave indications of the F phase, but the narrow existence

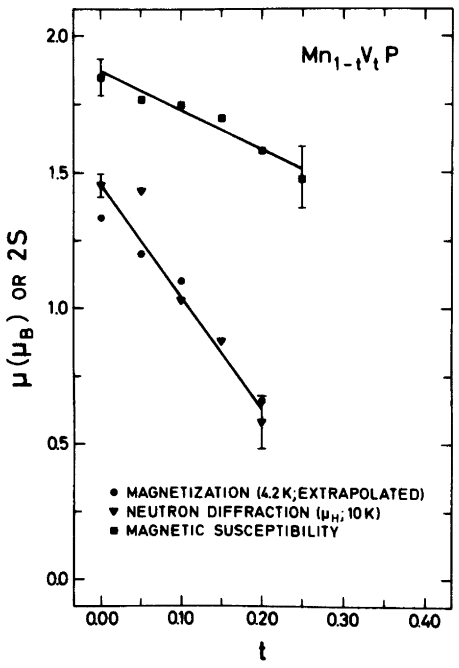

Fig. 5. Extrapolated magnetization moments (from Ref. 4), neutron diffraction moments (μ_H) and paramagnetic ("spin only") $2S$ values *versus* the compositional parameter t. Legends to symbols are given on the illustration. Bars represent estimated or calculated errors.

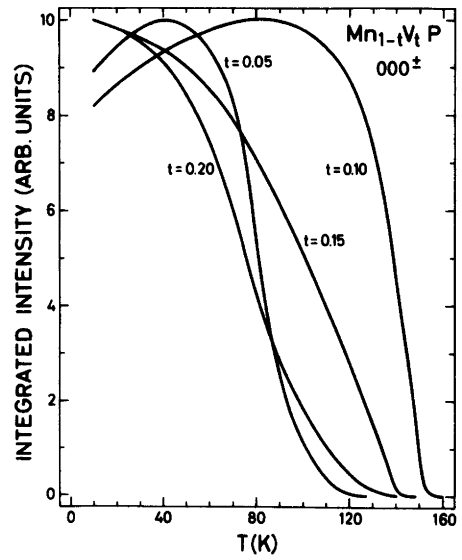

Fig. 6. Integrated intensity of $000^{\pm}$ *versus* temperature for $Mn_{1-t}V_tP$ with t=0.05, 0.10, 0.15 and 0.20. (H_c transforms to F for t=0.05 and 0.10 and to P for t=0.15 and 0.20.) Experimental points are omitted for clarity.

range from T_C=216±5 K[4] to T_S=152±5 K and μ_F<0.5 μ_B at 160 K prevents a more precise evaluation. No sign of the F phase was observed for t=0.15, 0.20 and 0.25.

The F to H_c phase transition is established for t=0.05 and 0.10, numerical values for T_S being given in Table 3. Although this transition is likely to be of first order (*cf.* Refs. 1, 2) no indication of hysteresis was observed in the temperature variation of the integrated intensity of the $000^{\pm}$ satellite for t=0.05 and 0.10 (Fig. 6). As is the case for all $Mn_{1-t}T_tP$ phases which we have studied[2,8] the temperature characteristics of the integrated intensity (I) of $000^{\pm}$ are rather broad. This applies also to the curves for t=0.15 and 0.20 in Fig. 6 which refer to the $H_c \rightleftarrows P$ transition (T_N is listed in Table 3). The origin of the maxima in I *versus* T for t=0.05 and 0.10 is not uncovered. A simple explanation would be that this behaviour reflects a temperature variation of the phase angle between the spirals. However, there are also other, and perhaps more likely, possibilities which cannot be tested before, say, single crystal

Table 3. Helimagnetic parameters for $Mn_{1-t}V_tP$ at 10 K. (R_{spiral} ranging between 0.04 and 0.08; 8–12 magnetic satellite reflections.)

t	$\tau_c/2\pi c^*$	μ_H (μ_B)	$\phi_{1,2}$ (°)	T_S (K)	T_N (K)
0.00	0.116±0.002	1.45±0.04	24±3	53±3	
0.05	0.118±0.002	1.43±0.06	40±10	102±5	
0.10	0.152±0.002	1.03±0.08	34±5	152±5	
0.15	0.189±0.002	0.88±0.10	42±10		140±5
0.20	0.195±0.002	0.58±0.14	70±20		113±5
0.25	H_c state not detected				

data come to hand. It may finally be appropriate to recapitulate from Ref. 4 that the H_c, F and P phases in the phase diagram of $Mn_{1-t}V_tP$ very likely meet in a triple point.

The original and simplest model[14,15] for the magnetic structure of the H_c phase of MnP was adopted for $Mn_{1-t}V_tP$. Numerical values for the variable parameters of the model (*viz.* the propagation vector τ_c of the spirals, the helimagnetic moment μ_H and the phase angle $\phi_{1,2}$ between the spirals through atoms 1 and 2, *cf.* Ref. 2) are listed in Table 3. The corresponding results for a powder sample of MnP are included in Table 3 for comparison (*cf.* also the discussion in Ref. 2).

The compositional variations of τ_c, μ_H and $\phi_{1,2}$ at 10 K are evident from Table 3 (*cf.* also Ref. 4). In order to determine the temperature variations of the parameters for a given t the positions and intensities of the satellites were examined at various temperatures. The τ_c *versus* temperature relationships (easily and accurately established) for t=0.00, 0.05, 0.10, 0.15 and 0.20 are shown in Fig. 7. As seen from the illustration τ_c undergoes a smooth, continuous variation with T, and the possibility of "lock-in" effects at integer numbers in the periodicity (*viz.* at $|\tau_c|^{-1}$ corresponding to 6, 7, 8 and 9 c edge lengths) can apparently be ruled out. Less decisive information is obtained for the temperature changes in μ_H and $\phi_{1,2}$. For t=0.10 (with T_S=152±5 K and T_C=216±5 K[4]) μ_H=0.8±0.1 μ_B and $\phi_{1,2}$=33±8° at 130 K. For t=0.15 and 0.20 (which do not undergo the H_c to F transition; *cf.* Ref. 4) μ_H is clearly continuously reduced to zero at T_N whereas $\phi_{1,2}$ appears to be maintained essentially unchanged from 10 K to T_N. (Approximate estimates for μ_H and $\phi_{1,2}$ could only be obtained at temperatures where μ_H remains approximately constant.)

No indication of any kind of co-operative magnetism has been obtained for t=0.25. In line with the findings in Ref. 4 we suggest that the SG region of the $Mn_{1-t}V_tP$ phase extends to t=0.25 (where the freezing temperature should be some 40 K). The border between the H_c and SG regions should accordingly be narrowed to $0.20<t<0.25$. A discussion of the SG regions in $Mn_{1-t}V_tP$ and $Mn_{1-t}Co_tP$ appears to require data over and above those available at the present time.

Acknowledgement. This work has received financial support from the Norwegian Research Council for Science and the Humanities.

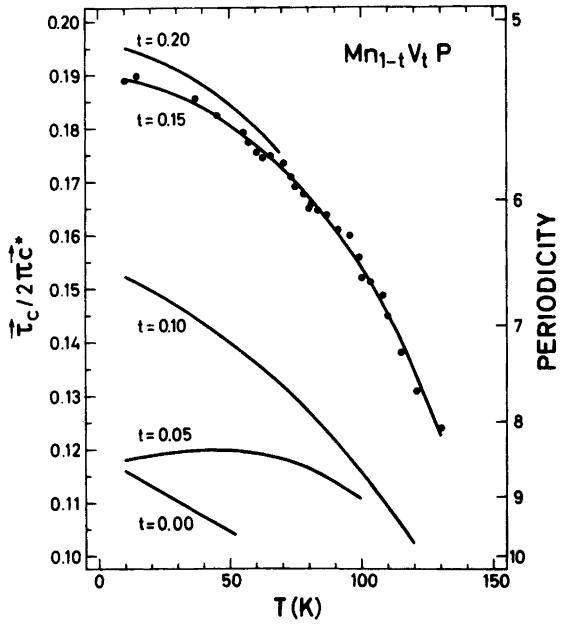

Fig. 7. Temperature dependences of the propagation vector (τ_c) for $Mn_{1-t}V_tP$ with t=0.00, 0.05, 0.10, 0.15 and 0.20. Experimental points are only shown for t=0.15.

REFERENCES

1. *Gmelins Handbook of Inorganic Chemistry, System No. 56: Manganese, Vol. C 9,* Berlin–Heidelberg–New York 1983.
2. Fjellvåg, H. and Kjekshus, A. *Acta Chem. Scand. A 38* (1984) 563.
3. Selte, K., Fjellvåg, H. and Kjekshus, A. *Acta Chem. Scand. A 33* (1979) 391.
4. Fjellvåg, H., Kjekshus, A., Zięba, A. and Foner, S. *J. Phys. Chem. Solids 45* (1984). *In press.*
5. Fjellvåg, H. and Kjekshus, A. *Acta Chem. Scand. A 38* (1984) 1.
6. Bacon, G. E. In Yelon, W. B., Ed., *Neutron Diffraction Newsletter,* Columbia 1977.
7. Watson, R. E. and Freeman, A. *Acta Crystallogr. 14* (1961) 27.
8. Fjellvåg, H. and Kjekshus, A. *Acta Chem. Scand. A 38* (1984). *In press.*
9. Selte, K. and Kjekshus, A. *Acta Chem. Scand. 27* (1973) 3195.
10. Endresen, K., Furuseth, S., Selte, K., Kjekshus, A., Rakke, T. and Andresen, A. F. *Acta Chem. Scand. A 31* (1977) 249.
11. Selte, K., Birkeland, L. and Kjekshus, A. *Acta Chem. Scand. A 32* (1978) 731.
12. Hiyamizu, S. and Nagamiya, T. *Int. J. Magn. 2* (1972) 33.
13. Kallel, A., Boller, H. and Bertaut, E. F. *J. Phys. Chem. Solids 35* (1974) 1139.
14. Felcher, P. G. *J. Appl. Phys. 37* (1966) 1056.
15. Forsyth, J. B., Pickart, S. J. and Brown, P. J. *Proc. Phys. Soc. 88* (1966) 333.

Received April 3, 1984.